X-ray diffraction topography using a diffractometer with a bendable monochromator at a synchrotron radiation source

D. Altin,[a]† J. Härtwig,[a]* R. Köhler,[b] W. Ludwig,[a] M. Ohler[a]‡ and H. Klein[a]§

[a]European Synchrotron Radiation Facility (ESRF), Grenoble, France, and [b]Humboldt Universität, Berlin, Germany. E-mail: haertwig@esrf.fr

The different properties of laboratory- and synchrotron-based double-crystal setups for X-ray topographic applications are discussed as a basis for the realization of a versatile instrument allowing the investigation of all kinds of crystals with high strain sensitivity and without any reduction in image size. It appears that the use of a bendable highly perfect monochromator (silicon) achieves this goal, through the local adaptation of Bragg angles, to compensate either dispersion or a bending of the sample.

Keywords: X-ray diffraction topography.

1. Introduction

X-ray diffraction topography is an imaging technique based on Bragg diffraction. It is used for the visualization of defects (*e.g.* dislocations, twins, domain walls, inclusions, impurity distributions) and macroscopic deformations (*e.g.* bending, acoustic waves) present within a single-crystal sample. It records components of long-range distortion fields connected with the defects or defect distributions as well as with macroscopic crystal deformation. Since the publication of the first X-ray topographic experiment (Berg, 1931), many different techniques have been created [see, for example, Lang (1978), Klapper (1991) and Bowen & Tanner (1998) for overviews of these techniques and their applications].

Double-crystal setups are used in X-ray topography to enhance strain sensitivity and to suppress background from radiation not used in image formation. Basically, two important groups of these setups exist: non-dispersive and dispersive ones. In practice, with laboratory sources, the non-dispersive setting is mostly used for topographical applications. One disadvantage of this non-dispersive setting is that in general the same material and the same reflection must be used for the monochromator/collimator (reference) and the sample crystal. With synchrotron radiation sources, the small angular source size in combination with the narrow spectral bandpass of the monochromator crystal yield nearly the same high strain sensitivity with dispersive and non-dispersive settings.

Besides strain sensitivity and the flexible choice of the reference crystal material, the achievable size of the image on the detector is an interesting parameter in double-crystal setups. With a laboratory source (not considering asymmetric reflections), the image dimension is practically equal to that of the source. One of the advantages of synchrotron radiation sources with their large source-to-sample distances is that images may be obtained that are much larger than the source size. However, the two setups behave differently. For a non-dispersive setting the image may achieve the dimension of the beam at the sample position, which in general is considerably larger than the source size. However, the aforementioned disadvantages concerning the material and reflections of the two crystals remain. In the case of a dispersive setting, the second crystal fulfils the Bragg condition only within a narrow band. Consequently, the diffracted beam (and the image) remains large in one direction but becomes narrow perpendicular to that direction.

This image-size limitation in a dispersive double-crystal setup may be overcome by a proper bending of the reference (monochromator) crystal. A local adaptation of Bragg angles (correction of dispersion) may be achieved, resulting in a large image in both dimensions (Kub, 1991). In this way, the non-dispersive and the dispersive (with Bragg-angle adaptation) settings give almost the same results for topography with respect to strain sensitivity, image size and the monochromator material. Thus, we may generally apply a dispersive setting by using the best available monochromator material, *i.e.* nearly perfect and easy-to-cool silicon. Consequently, one can investigate under optimum conditions practically all sample materials with the same monochromator, an adaptation of the monochromator to the sample material being unnecessary. In addition, a bent monochromator (or collimator) may be used to compensate for image shrinkage owing to the bending of a sample (Jenichen *et al.*, 1988).

In this work, we present some theoretical background and the technical realization of the aforementioned setup at the ESRF (Altin, 1999). The first results obtained with this instrument, which is now available to users, will also be presented.

2. Double-crystal topography

Let us recall the specific properties of double-crystal setups employed for topography at laboratory and especially at synchrotron sources, in order to discuss the strain sensitivity, the achievable size of the image on the detector and the possibilities of a flexible choice of the reference or monochromator/collimator crystal material. The properties of such setups may be analysed either graphically, using DuMond diagrams (DuMond, 1937), or analytically (Azaroff, 1974; Härtwig *et al.*, 1993). Here we will restrict ourselves to the ideas and conclusions useful for our discussion.

The diffracted intensity $I(\delta\Theta)$ or rocking curve in a double-crystal setup, as a function of the (global or local) misorientation angle $\delta\Theta$ of the second crystal, depends in an integral form on four functions: the spectral (S) and the angular (D) distributions of the incoming radiation and the reflectivity curves (according to the dynamical theory of X-ray diffraction) of the first ($R^{\rm I}$) and second ($R^{\rm II}$) crystal. We will consider the full width at half-maximum (FWHM) values in the θ space and/or in the λ space of these functions (w_S^θ, w_D^θ, $w_h^{\theta{\rm I}}$, $w_h^{\theta{\rm II}}$ and w_S^λ, w_D^λ, $w_h^{\lambda{\rm I}}$, $w_h^{\lambda{\rm II}}$, respectively). For a qualitative understanding, it is essential to remember that two 'divergences' should be considered: (i) the angular size of the source seen from one point of the crystal, which is related to the rocking curve and to the strain sensitivity (§2.1), and (ii) the angular aperture of the beam, often defined by slits, which is related to the dimension of the image on the detector (§2.2).

2.1. Strain sensitivity

The strain sensitivity is proportional to the slope of the intensity distribution $I(\delta\Theta)$ at the working point. For its estimation, it is useful to remember some analytical results.

In the case of an $(n,-n)$ setup and for both laboratory and synchrotron sources, the reflected intensity is to a very good approximation proportional to the autocorrelation function of the

† Present address: Siemens, München, Germany.
‡ Present address: Infineon Technologies AG, München, Germany.
§ Present address: CNRS, Grenoble, France.

 © 2002 International Union of Crystallography • Printed in Great Britain – all rights reserved

two identical reflectivity curves $R^{\rm I}$ and $R^{\rm II}$, and it does not depend on energy (non-dispersive setup). This function is very narrow (its width is of the order of that of the reflectivity curves $w_h^{\theta{\rm I}} = w_h^{\theta{\rm II}} \simeq 1$ arcsec) and, on the flanks, very steep. Consequently, in this case the highest strain sensitivities may be achieved. The practical problem is that to realize such a setting the monochromator crystal must be made from the same material as the sample crystal and the same reflection should be used. The monochromator should be a perfect crystal if the topograph is to show the defects of the sample and not those of the monochromator crystal. Owing to the very limited availability of crystals with sufficiently high perfection, this condition reduces the possible candidates for those highly sensitive settings to a limited number of substances.

In the case of the dispersive $(n,\pm m)$ setups and for laboratory sources, the situation is completely different. A laboratory source is often characterized by a large divergence ($w_D^\theta \simeq 1$ arcmin, defined by slits) and by a rather broad spectral line ($w_S^\theta \simeq 1$ arcmin, in the θ space), which are much larger than the widths of the reflectivity curves ($w_h^{\theta{\rm I}}$, $w_h^{\theta{\rm II}} \simeq 1$ arcsec). Now the reflected intensity appears to be, to a very good approximation, proportional to the spectral distribution S. Owing to its large width, the wide intensity distribution $I(\delta\Theta)$ has shallow flanks and the strain sensitivity is very low. This is why dispersive settings are not commonly used for topography in connection with laboratory sources. These limitations may be significantly reduced by decreasing the spectral width, for example, by using a collimator–monochromator combination like that of DuMond–Bartels (DuMond, 1937; Bartels, 1983).

At synchrotron sources, this disadvantage of dispersive $(n,\pm m)$ setups for X-ray topographical applications nearly vanishes. The small angular source size (often of the order of or even much smaller than the widths of the reflectivity curves $w_h^{\theta{\rm I}}$, $w_h^{\theta{\rm II}}$), in combination with the narrow spectral bandpass of the monochromator crystal, limits the spectral width of the beam after leaving the monochromator crystal to values close to the bandpass of usual sample crystals. In this way, the low divergent source acts like a pre-monochromator crystal in a dispersive setting. Now the reflected intensity is approximately proportional to the correlation function of the two reflectivity curves $R^{\rm I}$ and $R^{\rm II}$, resulting in a nearly non-dispersive setting. Consequently, high strain sensitivity is achieved even when using $(n,\pm m)$ setups, and it is reasonable to apply such setups to topography. Their major advantage is that we may use the best available monochromator material for the first crystal, namely highly perfect silicon. However, when using $(n,\pm m)$ setups at a synchrotron, one can be confronted with the limited dimension of the image on the detector.

2.2. Image dimension

For rather small source-to-sample and sample-to-detector distances, as in the laboratory case, the image dimensions in and perpendicular to the scattering plane are practically equal to that of the source (for symmetrical crystal reflections). Every part of a topograph is to a good approximation created by the same wavelength but coming from different points of the source (Figs. 1*a* and 1*c*). This fact does not change with the setup [that is, if $(n,-n)$ or $(n,\pm m)$ setups are used]. The image dimension within the scattering plane may be modified using asymmetric reflections. However, this limits the flexibility of the setup with respect to energy changes, which is often inconvenient in synchrotron work. Another possible way to increase the image dimensions in the scattering plane and perpendicular to it is to exploit the beam divergence and to increase considerably the source-to-sample distance (this applies to the laboratory and to the synchrotron case). Consequently, small and distant sources illuminate the different parts of the crystal with slightly different angles (Figs. 1*b* and 1*d*). Owing to the different angles under which the source shines on different crystal parts, the Bragg condition is fulfilled there for different wavelengths. The consequences of these changes are particularly important within the scattering plane.

For a non-dispersive setting, the second crystal simultaneously fulfils the Bragg condition for all these wavelengths. Consequently, the image (topograph) may be considerably larger than the source size, even within the diffraction plane. Its size is limited in both directions only by the beam divergence, which is considerably larger

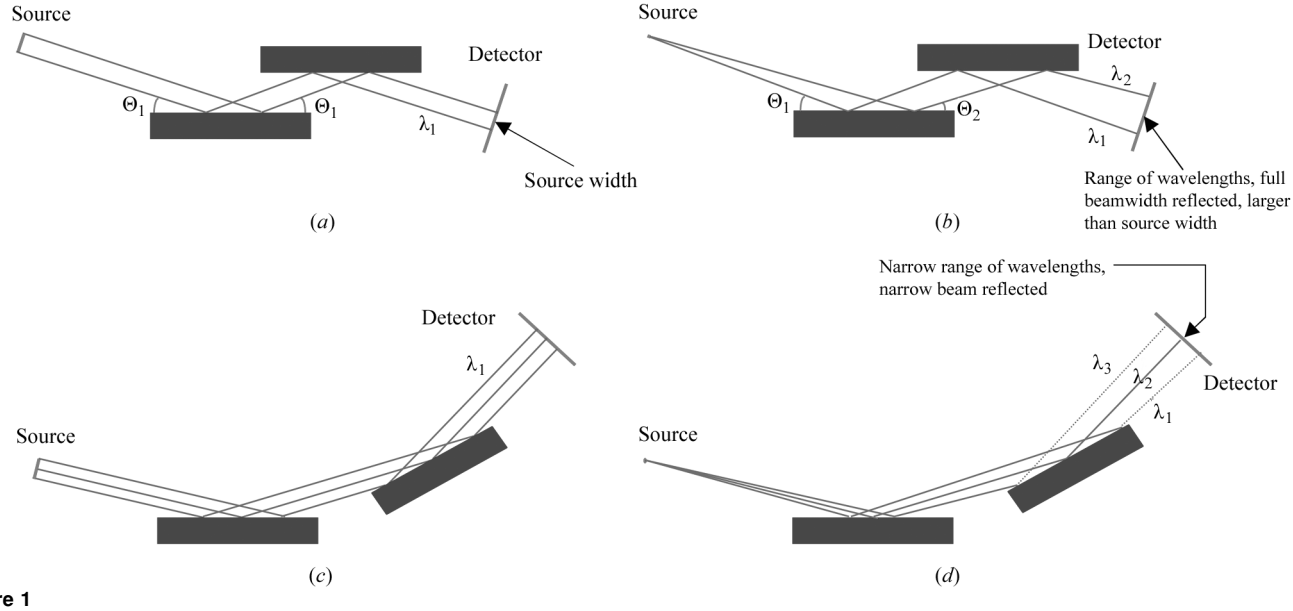

Figure 1
Schemes of several setups and for different kinds of sources: (*a*) $(n,-n)$ setup and close source (laboratory), (*b*) $(n,-n)$ setup and distant source (synchrotron), (*c*) $(n,+m)$ setup and close source (laboratory), and (*d*) $(n,+m)$ setup and distant source (synchrotron).

than the angular source size (*e.g.* of the order of 20 arcsec for the beam divergence and 0.2 arcsec for the angular size of the source when working at the ID19 150 m 'long' beamline at ESRF). The price for that enlargement is a change of wavelength (energy) along the image in the scattering plane and perpendicular to it. This changing wavelength in the topograph has practically no influence on the image contrasts.

This situation dramatically changes in the case of a dispersive setting. Now the second crystal fulfils the Bragg condition (in the dispersion plane) only within a narrow band. Consequently, the diffracted beam and the image remain large in the direction perpendicular to the diffraction plane, but become narrow in that plane (Fig. 1*d*).

2.3. Bendable monochromator

Our aim is to be able to use a unique double-crystal arrangement for all kinds of sample materials. The monochromator should be made out of the material with the highest degree of perfection, *i.e.* silicon, which in addition is rather easy to handle in the white beam (with respect to heat load, cooling *etc.*). We wish to have high strain sensitivity and a large image size. It is impossible to fulfil all these conditions with a plane monochromator crystal.

This problem may be overcome by a bending of the monochromator (Kub, 1991). In this way, we have a correction of dispersion or rather a local adaptation of Bragg angles. Thus, we may apply in general a dispersive setting with all its previously mentioned practical advantages. In addition, a bent monochromator (or collimator) may be used to correct the bending of a sample (Jenichen *et al.*, 1988). This is often necessary, for example, for wafers with superposed layers, commonly used for microelectronics applications. The general theoretical background of the discussed X-ray optical problem has been presented by Chukhovski *et al.* (1992). A discussion of image features in the discussed setups and in more general ones may be found in works by Servidori *et al.* (2001*a*,*b*).

The technical realization of the aforementioned setup was carried out at the ESRF. There we constructed, installed and tested a new double-crystal diffractometer with a bendable monochromator (Altin, 1999).

3. Examples of applications

The following examples show a comparison of results obtained with the most frequently used topographic technique using synchrotron radiation, the very simple and powerful white-beam topography, with double-crystal topographic results obtained with laboratory and synchrotron sources. In addition, further applications of double-crystal topography to different materials (related to various problems in materials science) are presented.

Fig. 2 shows a topograph of a quartz sample with a system of induced growth striations. It shows contrasts related to small misorientations of the order of 10^{-7} rad, induced by local variations of the impurity concentration (Bernhardt *et al.*, 1992). The topograph was taken with a laboratory double-crystal $(n,-n)$ setup, using a perfect strongly asymmetric quartz monochromator. In a white-beam topograph, this sample showed practically no contrast, because the strain sensitivity of that synchrotron technique is not high enough. A similar visibility may be achieved with a synchrotron double-crystal $(n,-m)$ setup, using a bendable perfect silicon monochromator (Fig. 3). The nominal monochromator curvature $R_{\rm I}$ needed to achieve Bragg-angle adaptation was calculated to be 2400 m. An absolute calibration of the bending mechanism is not necessary for the method to function. In the experiment, the form and dimension of the diffracted image was observed by a CCD video camera. The bending radius of the monochromator crystal was changed until complete (homogeneous) illumination of the diffraction image was obtained, which meant that the non-dispersive case had been achieved.

The bending radius $R_{\rm I}$ may be calculated using the results of Chukhovski *et al.* (1992), who considered the general situation of a non-dispersive case with two cylindrically bent crystals. For the special case with a flat second crystal, one obtains

$$R_{\rm I} = -\frac{L_{0\rm I}}{\sin\Theta_{0\rm I}}\left(1+\frac{1}{1-\tan\Theta_{\rm I}/\tan\Theta_{\rm II}}\right).$$

Here $L_{0\rm I}$ is the distance to the source of the first crystal, $\Theta_{\rm I}$ and $\Theta_{\rm II}$ are the Bragg angles of the first and the second crystal, and $\Theta_{0\rm I}$ is the angle of incidence (asymmetric cases possible) of the first crystal. Using the present experimental parameters, one obtains $R_{\rm I}$ = 2400 m for the monochromator curvature.

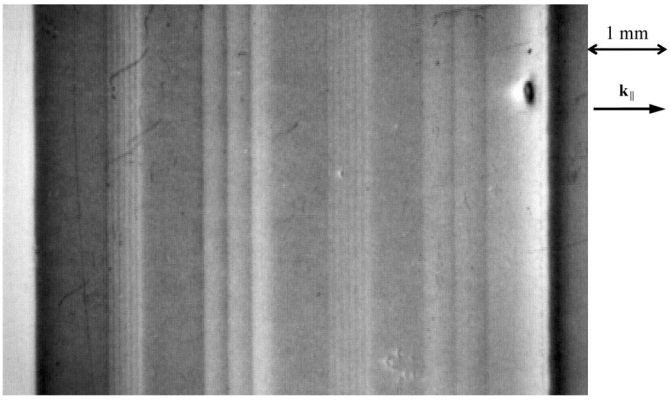

Figure 2
Plane-wave topograph of a quartz sample with induced growth striations, taken with a laboratory double-crystal $(n,-n)$ setup using a perfect strongly asymmetric quartz monochromator [both 4040 reflections (Bragg case, reflection geometry), Cu $K\alpha_1$ radiation, FWHM of the exit beam after the monochromator 0.16″, FWHM of the symmetrical sample reflection 0.91″, working point at 60% of the maximum intensity on the low-angle flank of the rocking curve]. The projection of the incident wavevector is indicated by $\mathbf{k}_{||}$.

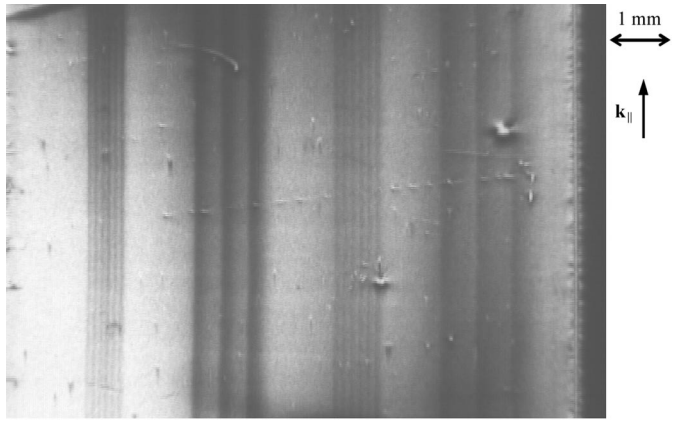

Figure 3
Double-crystal topograph of a quartz sample with induced growth striations, taken with a synchrotron double-crystal $(n,-m)$ setup using a bendable perfect silicon monochromator [asymmetric 448 monochromator reflection (asymmetry angle $\alpha = -17.6^\circ$) in the Bragg case, FWHM of the exit beam after the monochromator 0.31″, $80\bar{8}0$ sample reflection (Bragg case) with FWHM = 0.07″, but now on the high-angle flank of the rocking curve, E = 17.7 keV]. The projection of the incident wavevector is indicated by $\mathbf{k}_{||}$.

Fig. 4 shows the situation before and after the local Bragg-angle adaptation using a bendable monochromator to investigate a Lely-grown silicon carbide (4H-SiC) sample. In the case of the plane monochromator, the sample image is inhomogeneous, where the maximum of intensity is close to the upper corner of the topograph (Fig. 4*a*). With the proper bending, the image becomes (apart from the defects) homogenous. A further example is presented in Fig. 5, which shows a double-crystal topograph of a GaAs sample grown by the vertical gradient freeze technique (by J. Amon, B. Birkmann and G. Müller, Crystal Growth Laboratory, University of Erlangen, Germany). Several defects like an induced growth striation (related to variations of the silicon dopant concentration), the outcrops of a series of dislocations and polishing scratches are visible. In this case, the monochromator bending radius was $R_I = 800$ m.

As already said, it is possible by bending the monochromator to compensate not only for the dispersion of the setup but also for sample bending (Jenichen *et al.*, 1988). This is presented in the last example of a silicon sample with superposed test circuits. Fig. 6(*a*) shows the situation before the compensation for sample bending and dispersion (plane monochromator, bent sample), and Fig. 6(*b*) shows the state after it (bent monochromator, bent sample). In this way, a situation may be achieved where most parts of the sample diffract under equal conditions, that is, they have the same working point on

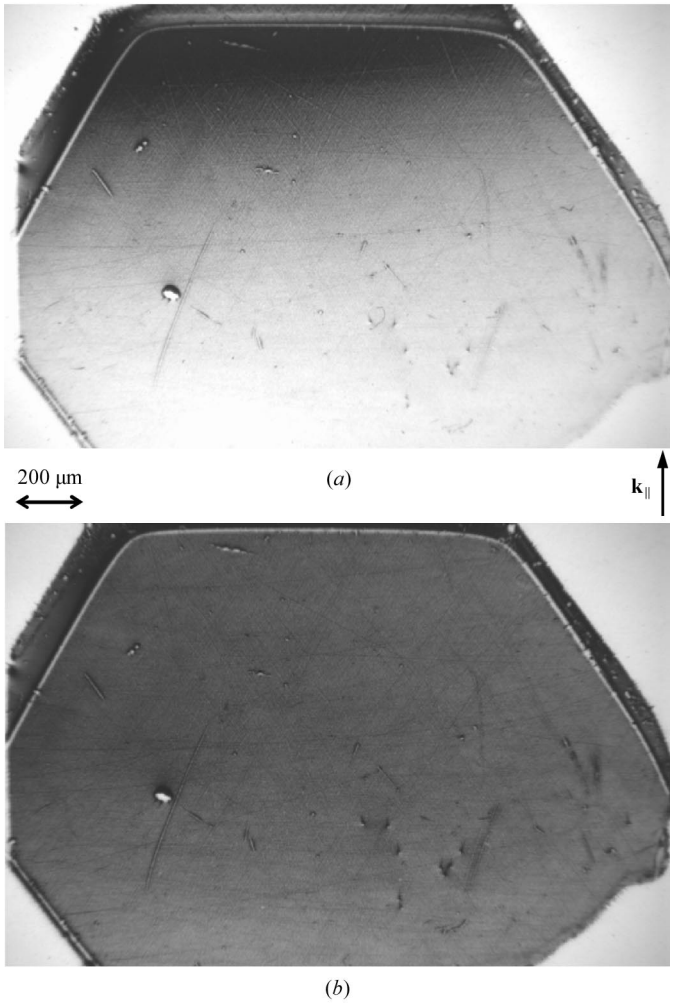

Figure 4
Double-crystal topograph of a Lely-grown silicon carbide (4H-SiC) sample, taken with a synchrotron double-crystal $(n,-m)$ setup using a bendable perfect silicon monochromator [symmetrical 333 monochromator reflection in the Bragg case, FWHM of the monochromator reflection 1.75″, $E = 8.7$ keV, symmetrical 0 0 12 sample reflection]: (*a*) before local Bragg-angle adaptation (plane monochromator, plane sample); (*b*) after local Bragg-angle adaptation (bent monochromator, plane sample).

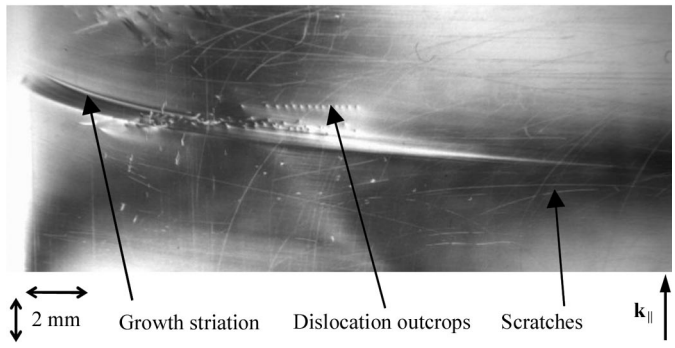

Figure 5
Double-crystal topograph of a GaAs sample with induced growth striations (grown by the vertical gradient freeze technique by J. Amon, B. Birkmann and G. Müller, Crystal Growth Laboratory, University of Erlangen, Germany), taken with a synchrotron double-crystal $(n,-m)$ setup using a bendable perfect silicon monochromator [asymmetric 448 monochromator reflection (asymmetry angle $\alpha = -17.6^\circ$) in the Bragg case, FWHM of the exit beam after the monochromator 0.31″, 880 sample reflection (Bragg case) with FWHM = 0.20″ on the high-angle flank of the rocking curve, $E = 17.4$ keV]. The projection of the incident wavevector is indicated by $\mathbf{k}_{||}$.

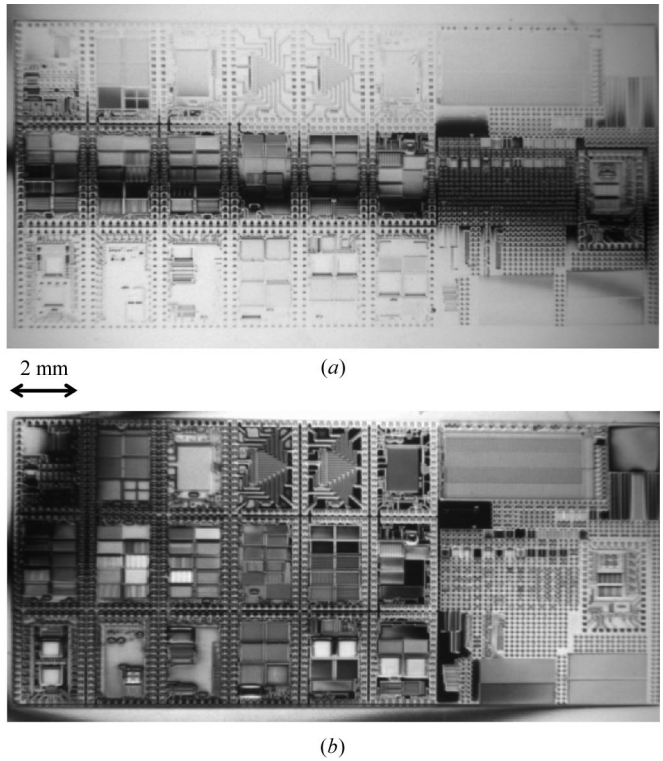

Figure 6
Double-crystal topograph of a silicon sample with superposed test circuits, taken with a synchrotron double crystal $(n,-m)$ setup using a bendable perfect silicon monochromator [symmetrical 444 monochromator reflection in the Bragg case, FWHM of the monochromator reflection 5.7″, $E = 11.58$ keV, symmetrical 008 sample reflection (Bragg case), FWHM 4.8″]: (*a*) before compensation of sample bending and local Bragg-angle adaptation (plane monochromator, bent sample); (*b*) after compensation of sample bending and local Bragg-angle adaptation (bent monochromator, bent sample).

the rocking curve (apart, of course, from the local deviations owing to the distortion fields).

4. Conclusions

A versatile double-crystal diffractometer for use at synchrotron sources was constructed to investigate samples of all kinds of crystalline materials with high strain sensitivity and without any reduced image sizes, but using only one monochromator material, namely that with the highest perfection (*i.e.* silicon). Meeting these demands became possible by using a bendable monochromator. In this way, in the very flexible dispersive setup, a local adaptation of Bragg angles or correction of dispersion may be achieved. In addition, a bent monochromator (or collimator) allows for the correction of sample bending.

The authors would like to thank José Baruchel, ESRF, Grenoble. Without his support the realization of the presented project would have been impossible. We thank René Chagnon and François Thurel for their high expertise in the field of mechanics and electronics and their enthusiastic contribution to this project.

References

Altin, D. (1999). *Reconstruction, Installation and Testing of a New Double Crystal Diffractometer with a Bendable Monochromator.* Diplomarbeit, Fachhochschule München.
Azaroff, L. V. (1974). *X-ray Spectroscopy.* New York: McGraw-Hill.
Bartels, W. (1983). *J. Vac. Sci. Technol.* B**1**, 338–345.
Berg, W. F. (1931). *Naturwissenschaften*, **19**, 391–396.
Bernhardt, Hj., Härtwig, J. & Lerche, V. (1992). *Prog. Cryst. Growth Charact.* **24**, 1–51.
Bowen, D. K. & Tanner, B. K. (1998). *High Resolution X-ray Diffractometry and Topography*. London: Taylor and Francis.
Chukhovski, F. N., Krisch, M. & Freund, A. (1992). *Rev. Sci. Instrum.* **63**, 920–923.
DuMond, J. W. M. (1937). *Phys. Rev.* **52**, 872–883.
Härtwig, J., Hölzer, G., Wolf, J. & Förster, E. (1993). *J. Appl. Cryst.* **26**, 539–548.
Jenichen, B., Köhler, R. & Möhling, W. (1988). *J. Phys. E*, **21**, 1062–1066.
Klapper, H. (1991). *Crystals: Growths, Properties and Applications, Band 13: Organic Crystals I: Characterization*, edited by H. C. Freyhardt & G. Müller, pp. 109–162. Berlin/Heidelberg: Springer Verlag.
Kub, J. (1991). *Phys. Status Solidi A*, **123**, 101–108.
Lang, A. R. (1978). *Diffraction and Imaging Techniques in Material Sciences*, edited by S. Amelinckx, R. Gevers & J. van Landuyt, pp. 623–713. Amsterdam: North-Holland.
Servidori, M., Cembali, F. & Milita, S. (2001*a*). *Appl. Phys.* A**73**, 75–82.
Servidori, M., Cembali, F. & Milita, S. (2001*b*). *Appl. Phys.* A**73**, 83–90.

 Received 18 January 2002 • Accepted 10 June 2002